INTERNATIONAL TABLES FOR CRYSTALLOGRAPHY

ISSN 1574-8707
it.iucr.org

Volume I, X-ray Absorption Spectroscopy and Related Techniques
ISBN: 978-1-119-43394-1

Chapter 3.26

In situ and *operando* catalysis: instrumentation and experimental setups

Giovanni Agostini,[a,b] Diego Gianolio[c]* and Carlo Lamberti[d,e]‡

[a]European Synchrotron Radiation Facility (ESRF), 6 Rue Jules Horowitz, BP 220, 38043 Grenoble, France, [b]Leibniz Institute for Catalysis at the University of Rostock (LIKAT), Albert-Einstein-Strasse 29A, 18059 Rostock, Germany, [c]Diamond Light Source Ltd, Harwell Science and Innovation Campus, Didcot OX11 0DE, United Kingdom, [d]Department of Chemistry, CrisDi Centre for Crystallography, University of Torino, Via Giuria 7, 10125 Torino, Italy, and [e]IRC 'Smart Materials', Southern Federal University, 5 Zorge Street, Rostov-on-Don 344090, Russian Federation. *Correspondence e-mail: diego.gianolio@diamond.ac.uk

‡ Deceased.

Keywords: catalysis; *ex situ*; *in situ*; *operando*; reaction cells; time-resolved setups; space-resolved setups.

The instrumentation and experimental setups needed to investigate catalysts by X-ray absorption spectroscopy (XAS) under *in situ* and *operando* conditions are briefly described. The relevance of the simultaneous collection of XAS data while monitoring the activity and selectivity of the catalyst (*operando* setups) is stressed and the compromises that are necessary to construct an *operando* cell are discussed. The same approach is used for cells that allow additional simultaneous data collection (X-ray powder diffraction, small-angle X-ray scattering, infrared, Raman or UV–visible). The role of time-resolved and space-resolved experiments is discussed, together with the need for sophisticated software that is able to handle a huge amount of XAS spectra coupled with other independent data collections.

1. Introduction and general considerations

The comprehension of and the correlation between catalytic performance, structure, electronic configuration and interaction of the catalyst, reactants and reaction intermediates are of paramount importance to improve the design of catalysts (Thomas, 1997). Due to the high dilution of the active species and the lack of long-range order typical of most catalysts, extended X-ray absorption fine structure (EXAFS) has been the technique of choice to understand the structure of the active sites, while the electronic configuration can be probed by X-ray absorption near-edge structure (XANES) and X-ray emission spectroscopy (XES) (Bordiga *et al.*, 2013; Borfecchia *et al.*, 2024; Boubnov *et al.*, 2014; Günter *et al.*, 2016; Lamberti & van Bokhoven, 2016).

To fulfil the need to operate under controlled temperature (T) and atmosphere, appropriate setups must be available at synchrotron-radiation beamlines. A typical setup for studying heterogeneous catalysts requires a cell where the catalyst, in a powdered or pelletized form, can be isolated from the external atmosphere. Such cells should allow both transmission and fluorescence detection (electron-yield detection is rarely used because of the poor electrical conductivity of most of the supports and the low mean free path of electrons in the presence of gases; Amakawa *et al.*, 2013; Escudero *et al.*, 2013; Hävecker *et al.*, 2009; Kristiansen *et al.*, 2013; Tamenori, 2013). In the case of experiments performed in transmission mode, the X-ray thickness of the sample must be optimizable, as for any XAS experiment. The cells must be compatible with accurate T and atmosphere control and allow the real-time study of catalyst activation and reactivity. A dynamic vacuum

Related chapters

Volume I: 2.22, 2.23, 3.14, 3.27, 8.10, 8.18

should be applicable to the cell and it should be capable of maintaining a static vacuum in the range 10^{-1}–10^{-4} mbar (depending on the sensitivity of the catalyst to air) for the time period needed to perform the experiment (up to 4 h for EXAFS spectra collected in fluorescence mode from diluted samples and up to 8 h for resonant inelastic X-ray scattering map detection). We differentiate among *ex situ*, *in situ* and *operando* experiments.

In situ experiments involve measurements of the catalyst under well controlled and static conditions (*T*, pressure and chemical composition) to investigate the structure of the active sites before and after interaction with probe molecules (Lamberti *et al.*, 2000; Valenzano *et al.*, 2012) or after interaction with reactants (Borfecchia *et al.*, 2015; Groppo *et al.*, 2008; Leofanti *et al.*, 2001, 2002; Muddada, Olsbye, Leofanti *et al.*, 2010), *i.e.* showing the reactivity of the active sites towards reactants.

The experimental setup needed for *operando* experiments is more demanding (Beale *et al.*, 2005; Boubnov *et al.*, 2014; Doronkin *et al.*, 2014; Ellis *et al.*, 2010; Frenkel *et al.*, 2012; Fulton *et al.*, 2007; Gamarra *et al.*, 2007, 2010; Hübner *et al.*, 2011; Janssens *et al.*, 2015; Kornienko *et al.*, 2015; Lamberti *et al.*, 2002; Lomachenko *et al.*, 2016; Muddada, Olsbye, Caccialupi *et al.*, 2010; Newton *et al.*, 2016; Paolucci *et al.*, 2016; Patlolla *et al.*, 2012; Rabeah *et al.*, 2016; Tada *et al.*, 2007; Yao *et al.*, 2014): gas-flow controllers are used to pass the desired gas feed with all of the reactants and the carrier gas needed for the reaction through the catalyst (for example C_2H_4, HCl and O_2 for an oxychlorination reaction or NH_3, NO and O_2 for an ammonia selective catalytic reduction reaction). *Operando* experiments are performed in flux, where a fraction of the gas outlet from the cell is sampled and sent to a quadrupole mass spectrometer (MS) for simultaneous evaluation of the catalyst performance (activity and selectivity; Grunwaldt *et al.*, 2005). The rapid response of MS analysis (1–20 s, depending on the number of sampled *m*/*q* ratios) is suited to time-resolved experiments, in which the catalyst temperature or the gas feed are changed. For steady-state experiments, MS should ideally be coupled to gas chromatography (GC), which guarantees a more accurate determination of the gas composition but requires longer times between two subsequent data collections, typically 10–20 min, which can be reduced to a few minutes with a micro-GC (Jian *et al.*, 2012; Xu *et al.*, 2016). Analysis of the gas outlet may also be performed by IR spectroscopy using appropriate gas cells. The use of toxic (CO, NO *etc.*), corrosive (NH_3, HCl *etc.*) flammable (H_2, C_2H_4, C_2H_2 *etc.*), oxidizing (O_2, O_3, NO_2 *etc.*) or asphyxiating (N_2, He *etc.*) gases requires particular care on chemical safety grounds. *Ex situ* experiments, which are used to analyze deactivated catalysts (Pellegrini *et al.*, 2011), are less demanding in terms of experimental setup as neither *T* nor atmosphere control is required.

For absolute energy calibration in real time, which is particularly relevant in the quantitative analysis of XANES spectra in redox catalysts, a third ionization chamber is necessary to monitor the edge of a reference sample (usually the corresponding metal foil; Lamberti, Bordiga *et al.*, 2003). This configuration is always possible for transmission setups, while in fluorescence setups it depends on the total absorption of the sample. When it is not possible to monitor the energy scale using a reference at the same time, the collection of a reference XANES spectrum before and after each catalytic experiment is highly recommended. Fig. 1 schematizes the typical experimental setup needed for XAS experiments in catalysis.

The next three sections describe the catalytic cells in more detail and underline the need to perform time-resolved and space-resolved experiments, reporting information on the corresponding setups and providing a list of beamlines where such instrumentation is available.

2. Cells allowing *in situ* and *operando* XAS and cells for simultaneous data collection with other vibrational (IR/Raman), electronic (UV–Vis, XES) or structural (SAXS, XRPD) techniques

Several authoritative reviews are available in the literature that describe cells for investigating catalysts under *in situ* and *operando* conditions using different spectroscopic and diffraction methods (Bare & Ressler, 2009; Bordiga *et al.*, 2013; Doronkin *et al.*, 2017; Grunwaldt *et al.*, 2004; Meunier, 2010).

The most common way to prepare powdered samples (such as heterogeneous catalysts) for XAS data collection is to press the material into a cylindrical pellet with a thickness and concentration that are optimized to obtain the best signal in transmission. For this reason, many XAS cells for catalysis have been designed to control *T* and gas atmosphere/pressure around the pressed disk (Dent *et al.*, 1992; Guilera *et al.*, 2009; Lamberti, Prestipino *et al.*, 2003; Sankar *et al.*, 2007; Tibiletti *et al.*, 2005; see Fig. 2*a*). This approach guarantees good homogeneity of the sample thickness, minimizing the consequences of minor movements of the beam on the sample during an EXAFS scan. The sample thickness can also be continuously tuned to optimize the signal-to-noise (S/N) ratio in the XAS spectra. This is the best solution for both *in situ* and *ex situ* experiments, but it is not ideal for *operando* experiments because the relatively low porosity of the pellet may suppress catalytic activity in the interior of the pellet. Also, reactant gases exiting the cell without interacting with the catalyst pellet may result in systematic errors in the evaluation of the

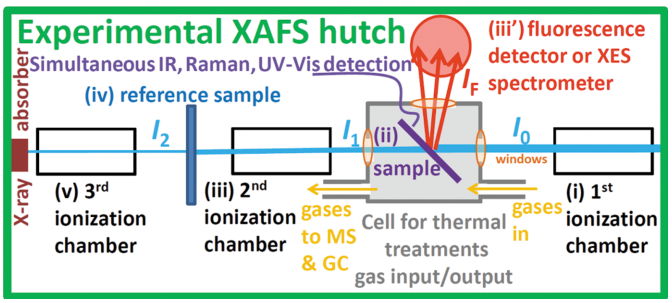

Figure 1
Typical setup for XAS experiments in catalysis. Adapted with permission from Bordiga *et al.* (2013). Copyright 2013 American Chemical Society.

catalyst activity/selectivity using MS and GC. This undesired effect can be minimized (but not eliminated) by designing cells with the smallest possible dead volume (*i.e.* the internal cell volume that is not occupied by the catalyst) and an optimized gas path. Such setups allow the collection of high-quality XAS data coupled with semi-quantitative catalytic data, and require standard catalytic tests to be repeated in the home laboratory for fully quantitative results. The alternative design reported in Fig. 2(*b*) forces the gas to diffuse through the entire cross section of a sample pellet (Meitzner *et al.*, 1998). The drawback of this setup, which is also used for IR spectroscopy (Lesage *et al.*, 2003), is that good porosity of the pellet is needed to minimize the pressure gap between the two sides of the cell. In some cases the porosity may be improved by mixing the catalyst with an inert phase that acts as a binder, such as alumina (γ-Al_2O_3), assuming that the catalytic properties of the sample are not altered (Doronkin *et al.*, 2017) and that the overall sample homogeneity is not compromised.

For online collection of quantitative catalytic data, the XAS cell must mimic a real catalytic reactor and this constrains the cell design. The simplest catalytic reactor that is compatible with *operando* XAS data collection is a capillary containing the catalyst (Fig. 2*c*), where reagents can be flowed in and the temperature can be controlled using a heat gun (Clausen *et al.*, 1991; Couves *et al.*, 1991). Glass, quartz, Kapton or metal capillaries can be used depending on *T*, pressure conditions and the X-ray energy range that is required for the experiment. This setup requires care to prevent the catalyst powder being flushed away by the reactant stream. Usually, glass-wool bundles are inserted into the capillary before and after the catalyst powder to prevent this problem.

Often, to achieve reliable comprehension of the system under investigation it is essential to characterize the catalyst under working conditions using multiple techniques (Borfecchia *et al.*, 2012; Jacques *et al.*, 2009). This means that XAS experiments should be complemented by other techniques that provide vibrational and electronic results in addition to XAS structural information. A discussion of whether complementary techniques should be performed in separate experiments or simultaneously with XAS data collection has been provided elsewhere (Lamberti *et al.*, 2016).

As discussed above, a cell for XAS measurements, and for spectroscopy in general, is not ideal for catalytic measurements because, besides optimizing the catalytic performance (the geometry of the catalytic bed and control of *T* and flow), it needs to allow the electromagnetic wave to probe the catalyst. Some of the difficulties that need to be overcome in cell design are feed impurities (for example an imperfectly sealed cell or degradation of the cell or some components), feed channelling and bed bypass, temperature gradients, X-ray beam effects, sample-preparation effects and catalytically active cell components *etc.* (Meunier, 2010). Other issues could arise from the necessity to control *T* in the catalytic bed, in particular for highly endothermic and exothermic reactions: Dilution of the sample with an inert and highly conductive solid is often not possible because it could decrease or alter the intensity of the spectroscopic signal. For instance, the optimal sample concentrations required for XAS and UV–Vis spectroscopy could be completely different and in some cases completely incompatible. The final point that we would like to highlight is the different volume and portion of the samples probed by each technique. This difference could be due to both the cell and the penetration depth of the different electromagnetic radiation inside the matter: for XAS it ranges up to millimetres, while for IR, for example, it only extends to a few hundred micrometres (Borfecchia *et al.*, 2017).

The choice of a catalytic cell, and more generally of the entire experimental setup and the measurement configuration,

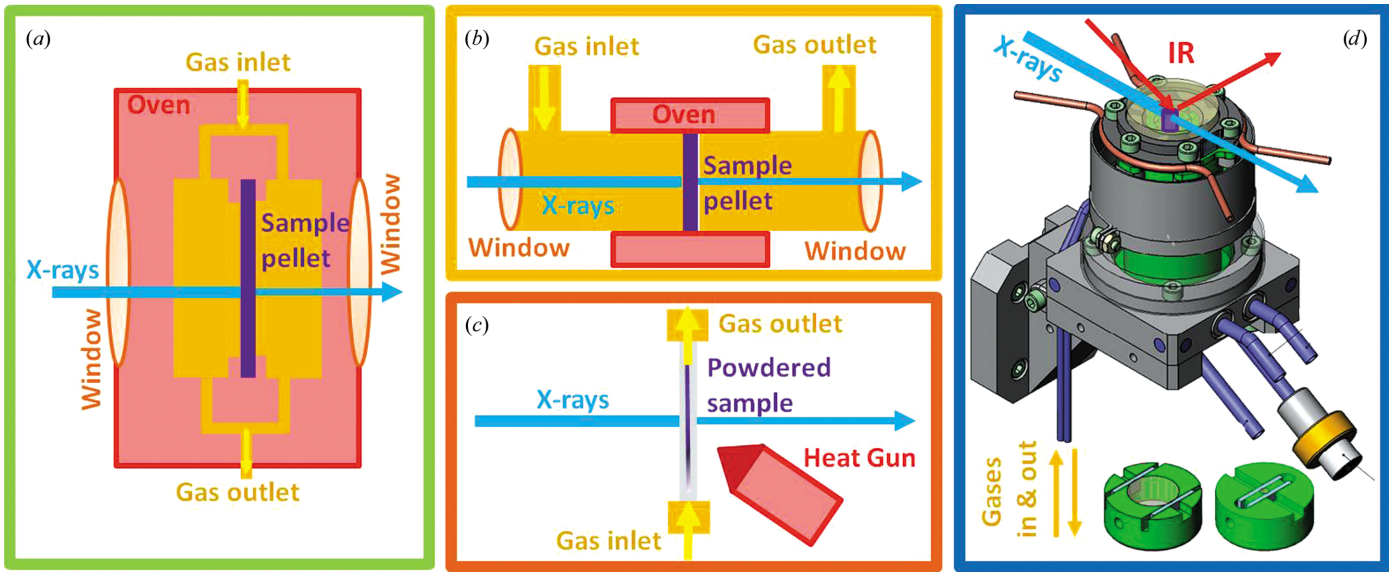

Figure 2
(*a*, *b*, *c*) Different designs of catalysis cells for XAS (see text for details). (*d*) Detailed view of the *operando* cell developed on BM23/ID24 at ESRF for simultaneous XAS measurements in transmission mode and IR spectroscopy in diffuse reflectance geometry. The bottom part shows two sample holders with two different thicknesses crossed by the X-ray beam. The top window is CaF_2.

suitable for the planned experiment will be driven by the scientific question. In planning an experiment, it will be necessary to clarify the priorities (time resolution, S/N ratio, temperature stability, combination of different techniques *etc.*), keeping in mind the advantages and drawbacks of each configuration (Grunwaldt *et al.*, 2004). Without any ambition to be exhaustive, some issues are underlined in the following paragraphs. The best data quality with equal time resolution is obtained by working in transmission mode on self-supported pellets with a cell devoted to XAS measurements (for example, the setups reported in Figs. 2*a* and 2*b*). As the setup moves away from this configuration, for example using a capillary system (Fig. 2*c*) or the addition of a second spectroscopy (Fig. 2*d*), a poorer S/N ratio is obtained. On the other hand, the capillary setup is a plug flow reactor and is the best solution for kinetic experiments since the gas feed passes through the whole powder with an almost plane wave and no dead volume is present. The time resolution achievable will be driven, from the spectroscopic point of view, by the minimum S/N ratio that is acceptable to collect a spectrum that is able to provide useful information. Of course, other parameters such as sample–reactant contact time, concentration *etc.* will affect the kinetic reaction. Moreover, the combination of different techniques often requires some compromise. For example, combined XAS–X-ray power diffraction (XRPD) experiments need to be designed to find the best compromise for the X-ray path both for the scattering and absorption techniques. Combination of XAS with IR spectroscopy requires an IR-transparent window (Fig. 2*d*), with consequent heat loss from the sample surface. In this case, accurate measurement of the temperature at the sample surface is necessary and the possible presence of a temperature gradient along the catalytic bed must be considered.

Historically, the first *operando* XAS–XRPD experiment was performed by the Topsøe group, who measured the activity and selectivity of binary Cu–Zn and ternary Cu–Zn–Al catalysts during reduction and water–gas shift and methanol synthesis, allowing the understanding of both the short- and long-range order of the active phase (Clausen *et al.*, 1991). Starting from this pioneering experimental setup, many variants were developed and produced (see, for example, Bordiga *et al.*, 2013; Chupas *et al.*, 2008; Figueroa *et al.*, 2013; Frenkel *et al.*, 2011; Meunier, 2010). The capillary system usually consists of a quartz capillary tube connected to a stainless-steel inlet and outlet by Swagelok tube fittings or glued directly to the tube. The outer diameter range is typically between 0.5 and 2 mm (to optimize μx and $\Delta\mu x$ for the sample), with a wall thickness of 0.01 mm. Depending on the setup, the capillary reactor is heated by exposing it to a stream of hot gas (N_2) produced by a heat gun (as represented in Fig. 2*c*) or by resistive wires placed close to the capillary. Temperature is controlled by a thermocouple within the capillary, located close to the catalyst, with a small diameter (below 0.2 mm) in order to minimize heat transfer without perturbing the gas flow. The capillary diameter, wall thickness and material can be varied according to the experimental requirements, in particular to work under high-pressure conditions where the thickness of the capillary walls needs to be increased. These setups are usually employed up to 1200 K and 20 bar (Figueroa *et al.*, 2013).

An interesting approach is the solution adopted at the SNBL beamline of the ESRF (BM01B, subesquently moved to BM31). This facility is equipped with two independent Si(111) monochromators (channel cut for XRPD and double crystal for XAS) and is capable of switching in less than a minute from a scattering to an absorption setup on the same sample and *vice versa*, always with the optimized and calibrated energy for both experiments (Abdala *et al.*, 2012; van Beek *et al.*, 2011).

Combined XAS–XRPD measurements can be performed by mounting a diffractometer in Debye–Scherrer geometry with the capillary microreactor mounted horizontally (x axis) and the diffracted X-rays detected in the xz vertical plane (where y is the direction of incoming photons) (Bras *et al.*, 2010). For XAS measurements, two ionization chambers are placed before and after the capillary to work in transmission geometry. If a fluorescence acquisition mode is needed, a solid-state detector is placed in the horizontal plane at 90° with respect to the direct beam (Fig. 1). In this case, in order to optimize the geometry configuration (to minimize the elastic beam and to maximize the solid angle between the catalyst and detector) the capillary system is rotated 45° with respect to incoming X-rays.

A further interesting development of the capillary setup for the investigation of the structure of catalysts under working conditions was performed on the BM26 beamline at ESRF (Beale *et al.*, 2006; Nikitenko *et al.*, 2008) using small-angle X-ray scattering (SAXS) techniques, probing large d-spacing, in addition to XAS and XRPD (also called WAXS). This setup is particularly suited to investigate samples during the synthesis process and is thus able to follow changes on scales ranging from nanometres to micrometres (Agostini *et al.*, 2014; Groppo *et al.*, 2012, 2014; Meneau *et al.*, 2003).

For the complete characterization of a catalyst beyond the structural information provided by scattering techniques such as WAXS and SAXS, vibrational and electronic spectroscopies are very powerful when coupled with XAS in order to investigate the active sites, the reaction intermediates and the catalyst surface (Baier *et al.*, 2015; Beale *et al.*, 2005; Bordiga *et al.*, 2015; Lamberti *et al.*, 2010; Newton *et al.*, 2004; Newton & van Beek, 2010). Two different types of cell will briefly be described in the following. The first type was originally developed by Beale and coworkers to combine Raman, UV–Vis and XAS in an energy-dispersive configuration (Beale *et al.*, 2005). It is based on a quartz capillary. Raman and UV–Vis measurements can be carried out by irradiating and collecting the signal using a fibre optic, which can be inserted and placed in front of the catalyst quite easily. The use of a capillary reactor could give rise to issues derived from the round shape of the quartz reactor, which may alter the signal back-reflected to the probe. These problems can be overcome by making flat faces in the direction perpendicular to the incoming radiation, grinding a reactor tube (6 mm outer diameter and 1 mm inner diameter) made of optical grade quartz glass. The reactor is

mounted in a square stainless-steel furnace and heated by four cartridges, with a maximum usable temperature of 920 K. The second type of cell is based on the idea of Evans and Newton to combine XAS with IR spectroscopy collected in diffuse reflectance (DR) mode (Newton *et al.*, 2004). The cell is designed to be as close as possible to a plug flow reactor, with the sample in powder form and the gas feed passing through the catalytic bed. XAS measurements are performed in transmission geometry (which is compatible with both standard and energy-dispersive modes), while the IR spectrum is collected in DR geometry (Fig. 2*d*). A series of crucibles with different diameters to host the powder sample are available in order to be able to optimize the X-ray path as a function of the metal loading and the energy of XAS measurements in transmission mode (Fig. 2*d*, bottom). The cell is windowed with two carbon glass plates for X-rays and with a CaF_2 crystal on top for IR. Recently, this cell was updated by the BM23/ID24 staff at the ESRF, maintaining the same geometrical configuration from IR spectroscopy but redesigning the whole cell to minimize the dead volume to 0.5 cm^3, in order to measure both in transmission and fluorescence geometries and to work up to 970 K at a pressure of 10 bar (Fig. 2*d*).

Due to space limitations, this short review is focused on heterogeneous catalysts measured with hard X-rays. For the experimental setups used to investigate catalysts in the soft X-ray regime, we refer to Chen (1997), Hävecker *et al.* (2009), Somorjai *et al.* (2011) and Toyoshima & Kondoh (2015), while for homogeneous catalysis we just mention that stopped-flow cells (Gomez-Hens & Perez-Bendito, 1991; Inada *et al.*, 1997) have been widely employed to investigate the time evolution of chemical reactions in the liquid phase by time-resolved XAS (Bartlett *et al.*, 2011, 2014; Dent *et al.*, 1999; Guilera *et al.*, 2006; Oyanagi *et al.*, 2011; Abdul Rahman *et al.*, 2003; Smolentsev *et al.*, 2009).

3. Time-resolved data collection

Timescales in homogeneous and heterogeneous catalysis range from milliseconds (nucleation and growth, sintering and particle morphology changes) to seconds (reaction-turnover times) to minutes (reduction and oxidation reactions) to hours or days (catalyst deactivation, degradation and ageing).

From its very earliest days, measuring a standard EXAFS spectrum in transmission mode has required about 1 h. With

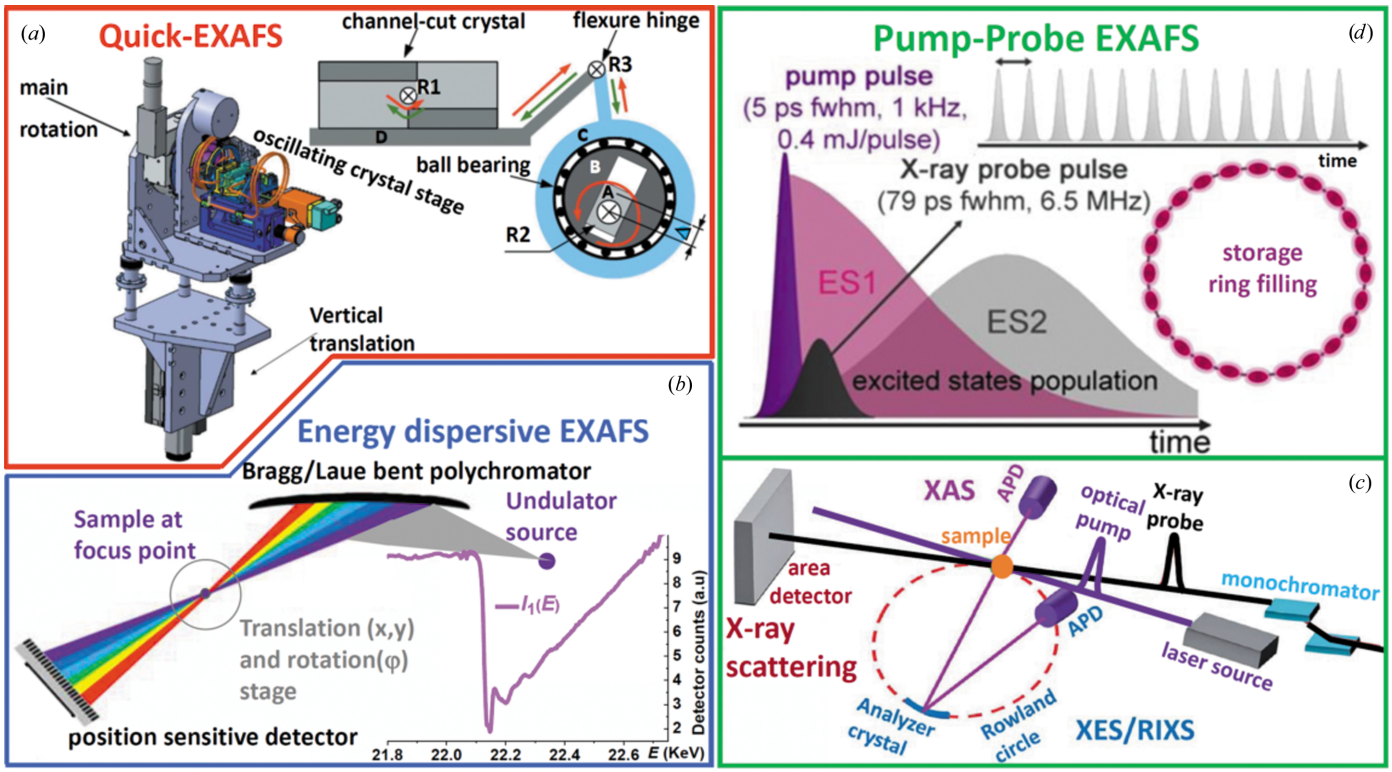

Figure 3
(*a*) Scheme of the SAMBA quick EXAFS monochromator at the SOLEIL synchrotron. The main rotation stage selects an average Bragg angle and the oscillating crystal stage produces fast oscillation around this value. Adapted with permission from Fonda *et al.* (2012). (*b*) Left: scheme for an energy-dispersive EXAFS setup. The polychromatic beam is diffracted by a bent crystal, focused on the sample and then diverges towards a position-sensitive detector where the beam position is correlated to energy, resulting in a single-shot I_1 spectrum (right). Adapted with permission from Bordiga *et al.* (2013). Copyright 2013 American Chemical Society. (*c*) Scheme for a combined pump–probe XAS (violet APD), XES (analyzer crystal and blue APD) and X-ray scattering (area detector) experiment; the laser and X-ray pulse arrive on the sample at different times, allowing excited states of the system to be probed. Adapted from Chen *et al.* (2014) with permission from the Royal Society of Chemistry. (*d*) Top right: schematic representation of the space occupancy of electron bunches in the storage ring and the consequent time structure of the X-rays emitted by synchrotron sources. Bottom left: scheme of the time population of two hypothetical excited states (ES1 and ES2) of a typical metal complex upon laser excitation (violet peak). By changing the delay between the laser pulse and the X-ray probe (black peak), the nature and the time evolution of the excited states can be revealed.

this standard setup, the spectrum was built up by collecting each data point at a fixed energy, with the monochromator stationary in angle (step-scan mode). When the desired collection time per point was reached, the monochromator was then moved to select the next energy and the measurement was repeated step by step until the whole energy range was covered. Whilst this is still a popular mode of data collection (and indeed produces accurate data in many cases), the overheads of moving and settling the monochromator make it difficult to follow a chemical reaction in real time. Indeed, for very low acquisition times per point, the scan time will be dominated by the dead time taken to move from one point to the next. More recently, technological advances have improved the time resolution to fractions of a second with 'on-the-fly' or quick EXAFS (Q-EXAFS; Nachtegaal *et al.*, 2016) and to milliseconds with energy-dispersive EXAFS (ED-XAS; Mathon *et al.*, 2016), allowing the use of *operando* experiments under non-equilibrium conditions.

Q-EXAFS, or 'on-the-fly XAS', removes the time overheads associated with step scanning by continuously moving a double-crystal or channel-cut monochromator through the energy range of interest at a constant speed, while the detectors and Bragg motor encoder are sampled simultaneously at regular time intervals that will define the energy resolution (step size). This mode was first introduced by Frahm at the RÖMO II beamline at HASYLAB (Frahm, 1988), and has now been implemented on many beamlines around the world such as, for example, BW1 (Richwin *et al.*, 2001) at HASYLAB, SNBL (Abdala *et al.*, 2012), BM29 (Prestipino *et al.*, 2011), BM23 (Mathon *et al.*, 2015) and DUBBLE (Nikitenko *et al.*, 2008) at ESRF, B18 at Diamond Light Source (Dent *et al.*, 2013), BL01 at SPring-8 (Tada *et al.*, 2007), SuperXAS at SLS (Müller *et al.*, 2016) *etc*. Dedicated Q-EXAFS systems have been implemented with technical details that allow subsecond resolution to be reached for a full EXAFS scan. This holds for a concentrated sample such as a metal foil, while on a catalytically relevant diluted sample a scan can routinely be acquired in a minute or less, or in a few seconds if the measurement is limited to only the XANES region.

The Q-EXAFS instrumentation, which allows high-performance time resolution, is characterized by a channel-cut crystal monochromator that moves in an oscillatory motion driven by an actuator with a frequency of up to 50 Hz around a preselected Bragg angle and by a data-acquisition system that simultaneously samples several detectors and encoders (Fig. 3*a*). This kind of monochromator has been installed on the SuperXAS beamline at the SLS (Müller *et al.*, 2015), and other versions can be found on X18A and X18B (Khalid *et al.*, 2011) at the NSLS (Brookhaven) and on BL33XU at Spring-8 (Uruga *et al.*, 2007). The monochromator initially installed on the SAMBA beamline at the SOLEIL synchrotron (Fonda *et al.*, 2012; see Fig. 3*a*) has since been moved to the ROCK (Briois *et al.*, 2016) beamline at the same synchrotron and will be briefly commented on. A vertical motorized stage (left) performs the main rotation; this is necessary to align the oscillating crystal stage with an average Bragg angle. The oscillating stage produces the fast oscillation and controls its amplitude. The scheme on the right illustrates the working principle of the variable cam. A coupling system allows the transmission of a rotating motion through a flexure hinge to the monochromator crystals without mechanical play. This system allows frequencies of tens of hertz to be reached for scan collection. The drawback of Q-EXAFS monochromators is that they do not have a fixed exit, resulting in movement of the beam with respect to the sample during the energy scan. This means that a larger energy scan would result in a higher position shift of the X-ray beam on the sample, which is particularly relevant in the low-energy region (Ti, V and Cr *K* edges), where larger $\Delta\theta_{\rm Bragg}$ are required for the same ΔE.

In the Q-EXAFS mode the data are still collected in a serial manner, which ultimately limits the speed. A completely different approach is energy-dispersive XAS or ED-XAS. The ED geometry (Pascarelli *et al.*, 2016) uses a bent monochromator crystal (Allen *et al.*, 1993; Hagelstein *et al.*, 1995), where the variation of the diffraction angle over the crystal surface can be assumed to be linear. Depending on the illuminated length and Bragg angle a specific energy range is diffracted. The sample under investigation is located at the focal point of the monochromator (Fig. 3*b*), and the intensity of the different diffracted energies is measured by a position-sensitive detector (Oyanagi *et al.*, 1986). At each channel of this detector an energy interval is then attributed following a careful calibration process (Ruffoni & Pettifer, 2006). Thus, one can take repeated snapshots of the entire EXAFS spectrum on a timescale of few microseconds, limited only by the detector readout time and the photon flux. On diluted samples, as relevant in catalysis, the actual time resolution is usually in the millisecond range.

Historically, the use of ED-XAS started almost 40 years ago at the II-4 beamline of SSRL, with a collaboration between scientists from Stanford and from the Photon Factory in Tsukuba (Kaminaga *et al.*, 1981; Matsushita & Phizackerley, 1981; Phizackerley *et al.*, 1983). Successively, this technique has spread to many other synchrotron sources, for example the Photon Factory in Japan (Saigo *et al.*, 1986), the D11 beamline at the DCI storage ring of LURE (Dartyge *et al.*, 1986; Flank *et al.*, 1982, 1983), the DEXAFS station of the DESY storage ring in HASYLAB (Hagelstein *et al.*, 1989), the SRS in Daresbury (Allinson *et al.*, 1988; Dent *et al.*, 1999), the EXAFS-PULS beamline at the ADONE synchrotron in Frascati (D'Acapito *et al.*, 1992) and the X6A beamline at the NSLS (Lee *et al.*, 1994). Several ED beamline are now available worldwide, among them ID24 at the ESRF (Pascarelli *et al.*, 2016), I20 at Diamond Light Source (Diaz-Moreno *et al.*, 2009), ODE at SOLEIL (Baudelet *et al.*, 2011), D06A at LNLS (Cezar *et al.*, 2010), BL08 at Indus-2 (Bhattacharyya *et al.*, 2009), BL2.2 at SLRI (Poo-arporn *et al.*, 2012) and the ED beamline of the Kurchatov Synchrotron Radiation Source in Moscow (Aksenov *et al.*, 2006).

Despite this high time resolution, two main problems restrict the applications of ED-XAS. Firstly, spectral normalization and compensation with respect to I_0 are an issue due to beam instability in flux and position and to homogeneity of

samples. Secondly, the ED geometry is efficient in the transmission geometry configuration only. Both drawbacks can be partially overcome by scanning a narrow slit of few tens of micrometres through the polychromatic fan of radiation downstream of the crystal and selecting a monochromatic beam, the intensity of which is simultaneously recorded before and after the sample by two ionization chambers, while the fluorescence emitted by the sample is simultaneously collected by a standard multi-element solid-state detector (Pascarelli *et al.*, 1999). The cost of this setup is that the time resolution is driven by the slit scan (typically hundreds of milliseconds). An *ad hoc* catalytic cell has been developed for this specific setup (Guilera *et al.*, 2009) and some relevant results have been obtained (see, for example, Nagai *et al.*, 2008).

For the time-resolved characterization of photocatalysis, ultrafast pump-and-probe spectroscopic methods are also relevant in order to probe photo-induced structural and electronic dynamics on timescales in the microsecond to picosecond range at third-generation synchrotrons, and potentially on the femtosecond scale at XFEL sources. These methods are based on the response to an external excitation (primarily laser pulses for photocatalysts, but also heat, magnetic field *etc.* for different systems) and the measurements are performed in differential mode by means of pump–probe schemes (Borfecchia *et al.*, 2013; Bressler & Chergui, 2004, 2010; Chen, 2004; Milne *et al.*, 2014; see Fig. 2*c*). Transient difference signals (between the excited and ground state) are recorded for each energy point and the spectrum is then built up; several repetitions are typically needed to improve the signal-to noise ratio. Different setups have been developed to monitor X-ray absorption, emission and scattering processes and to cover the whole temporal range (Chen *et al.*, 2014).

To collect XAS on photo-active systems in the solution phase on the microsecond timescale, the pump–flow–probe method can be employed. Here, the liquid samples flow through a jet and the technique exploits the spatial separation between the spot where the two beams (laser excitation and X-ray probe) hit the sample, so that the time delay is defined by the speed of the liquid sample and the spatial separation between the two beam spots. A setup for pump–flow–probe measurements exists at the SuperXAS beamlines (Smolentsev *et al.*, 2013). As opposed to pump–flow–probe methods, conventional pump–probe setups exploit the temporal structure of the X-ray beam at a synchrotron (top right corner of Fig. 3*d*), and the highest resolution (femtoseconds) can only be achieved at X-ray free-electron lasers or slicing sources at synchrotrons since it is limited by the duration of the X-ray pulse (bottom left corner of Fig. 3*d*). The time delay between the laser pump and X-ray probe can be tuned electronically by gating the detector or mechanically by chopping the X-ray beam (with the second method having the advantage of reducing the X-ray damage since the sample is only irradiated for the measurement). Laser pump–X-ray probe setups exploiting the temporal structure of the X-ray source (top right corner of Fig. 3*d*) have been developed at third-generation synchrotrons. Among the different available beamlines we mention 7-ID-D (March *et al.*, 2011) and 11-ID-D (Chen *et al.*, 2010; Jennings *et al.*, 2002) at APS, Chicago, USA, MicroXAS (Lima *et al.*, 2011) at SLS, Villigen, Switzerland, P11 (Britz *et al.*, 2016; Göries *et al.*, 2016) at PETRA III, Hamburg, Germany and NW14A (Sato *et al.*, 2009) at the Photon Factory, Tsukuba, Japan. In recent years the new hard X-ray free-electron laser (FEL) sources have boosted the physics and chemistry of time-resolved experiments, providing ultrahigh fluxes of up to $\sim 10^{12}$ photons per pulse (compared with 10^{6} photons per pulse at third-generation synchrotrons) and extreme short length (tens of femtoseconds, compared with hundreds of picoseconds). Pump-and-probe experiments at FELs can be performed at SACLA in Japan (Canton *et al.*, 2015; Ishikawa *et al.*, 2012), at the XPP endstation of the LCLS in Stanford (Cammarata *et al.*, 2014; Harmand *et al.*, 2013) and at the FXE endstation of the European XFEL, Hamburg, Germany.

4. Spatially resolved data collection

In tandem with the temporal resolution, another important property of synchrotron-based techniques is the considerable spatial resolution that is achievable at these facilities (Martinez-Criado *et al.*, 2013; Mino *et al.*, 2018; Suzuki & Terada, 2016). The capability to focus the beam and map different points of the sample has been thoroughly exploited by X-ray fluorescence (Kalirai *et al.*, 2015), imaging (Andrews & Weckhuysen, 2013; Aramburo *et al.*, 2013) and tomography (Gonzalez-Jimenez *et al.*, 2012; Grunwaldt & Schroer, 2010; Meirer, Kalirai, Weker *et al.*, 2015), but it also has a relevant application in the case of the EXAFS technique, in particular when applied to catalysis studies, since it allows characterization of the axial structural variance of working catalysts along a reaction bed (Doronkin *et al.*, 2014; Grunwaldt *et al.*, 2013; Günter *et al.*, 2016; Hannemann *et al.*, 2007, 2009; Kimmerle *et al.*, 2009). The absence or presence of such structural gradients is of considerable interest in the realistic application of heterogeneous catalysts and is not easily established in any other way. Certainly, the possibility of performing time-resolved and space-resolved measurements (Doronkin *et al.*, 2014) is strictly connected to the development of *in situ* cells that allow reaction environments to be reproduced that are as close as possible to those that the catalysts would experience under actual working conditions. Several adjustments in terms of scale and materials are required to make the cell compatible with X-ray absorption measurements: thin windows of a material mainly composed of light elements (Kapton, Mylar, glassy carbon, mica *etc.*) to optimize transmission that is possibly not crystalline and with a negligible amount of impurities to minimize unwanted spurious diffraction or scattering or fluorescence signals that would introduce systematic artefacts into the measurement.

Capillary-like cells (Figs. 2*c*, 4*a* and 4*b*) offer ideal conditions in terms of gas/liquid flow, temperature range and pressure resistance, providing a great tool for an improved full structural characterization of catalysts, so many groups started to develop custom-built *in situ* cells based on plug flow capillary reactors (Bare *et al.*, 2007; Fiddy *et al.*, 1999; Newton

et al., 2003). Moreover, the capillary provides a linear environment for gas/liquid flow and good accessibility to different points of the catalyst bed, allowing space-resolved measurements that are capable of discerning differences between the start and the end of the catalytic bed, where the gas/liquid composition can be very different depending on the rate of reactant consumption and product formation (Newton *et al.*, 2016). If the temporal resolution for data acquisition is sufficiently higher than the reaction rate, it is also possible to monitor progress along the bed of the reaction front. A possibility is to loop on the different points of the catalytic bed (from 1 to *n* in Fig. 4*a*; Doronkin *et al.*, 2014); alternatively, a full-field approach (Andrews & Weckhuysen, 2013; Grunwaldt & Schroer, 2010; Meirer, Morris *et al.*, 2015) must be adopted.

A nanoreactor originally designed for environmental high-resolution transmission electron microscopy (TEM) was adapted for scanning transmission X-ray microscopy (STXM) on beamline 11.0.2 (Kilcoyne *et al.*, 2003) of the ALS synchrotron at BNL operating in the soft X-ray region (see Fig. 4*c*). This setup has provided several very interesting results for understanding catalysts under working conditions; see, for example, de Smit *et al.* (2008). Beamline 37XU (Terada *et al.*, 2011) at SPring-8 is an example of an STXM setup operating in the hard X-ray region that is widely employed by the catalysis community (Tada *et al.*, 2011).

Finally, using microfocus X-ray fluorescence and X-ray diffraction computed tomography (μ-XRF-CT and μ-XRD-CT, respectively) in combination with XANES on a single particle of a catalyst it is possible to study the active state under standard operating conditions, demonstrating the ability of chemical computed tomography to image the nature and the spatial distribution of a single catalyst particle under

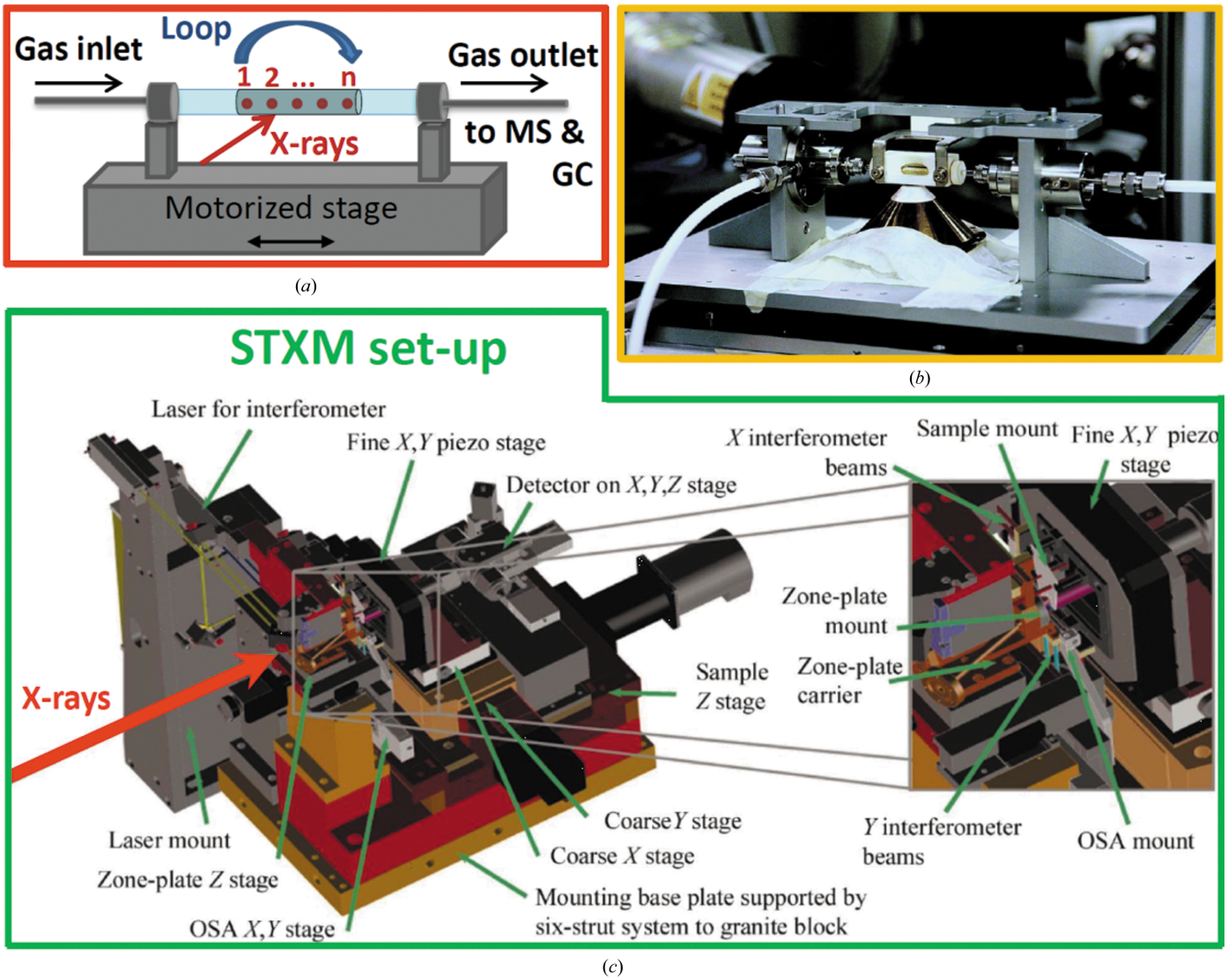

Figure 4
Schematic (*a*) and photograph (*b*) of the capillary reactor available at the Diamond Light Source beamlines. The setup is equipped with Swagelok fittings to flow gases through the sample and a hot air blower to control the temperature and is mounted on a motorized stage, allowing the possibility of probing different points along the catalyst bed. (*c*) Three-dimensional drawings of the 5.3.2 STXM beamline at the ALS synchrotron. Reproduced with permission from Kilcoyne *et al.* (2003).

reaction conditions (Cats *et al.*, 2013; Liu *et al.*, 2016; Meirer, Kalirai, Morris *et al.*, 2015; Meirer, Morris *et al.*, 2015; Price, Geraki *et al.*, 2015; Price, Ignatyev *et al.*, 2015).

5. Conclusions

In recent years, impressive achievements have been obtained in the development and adaptation of spectroscopic techniques for *in situ* and *operando* studies of processes under real and close-to-real reaction conditions. Synchrotron-based XAS has emerged as one of the most used methods for the study of active sites in catalytic materials (Bordiga *et al.*, 2013). Excellent spatial, temporal and energy resolution and the relatively high penetration depth of hard X-rays make it a perfect tool to investigate systems under reaction conditions (gas atmosphere or pressure, sample temperature) and to probe catalytic processes during the reaction (Buurmans & Weckhuysen, 2012; Grunwaldt *et al.*, 2004; Grunwaldt & Clausen, 2002; Newton *et al.*, 2002). The huge amount of data obtained by time-resolved or space-resolved data collection (and using multi-technique experiments) has generated the need for a new generation of software allowing the simultaneous handing of a large number of spectra and their treatment with advanced chemometric approaches such as principal component analysis (Cotte *et al.*, 2016; Figueroa & Prestipino, 2016; Liu *et al.*, 2012). When additional techniques (MS, GC, XRPD, SAXS, IR, Raman, UV–Vis *etc.*) are coupled with XES or XAS acquisitions, we foresee the need to drive all data collections with a single computer to allow perfect timing among the different data sets.

Acknowledgements

CL thanks the Russian Ministry of Education and Science for support (megagrant No. 14.Y26.31.0001). The authors are indebted to Elisa Borfecchia (Haldor Topsøe A/S, Denmark) for critical reading of the manuscript.

References

Abdala, P. M., Safonova, O. V., Wiker, G., van Beek, W., Emerich, H., van Bokhoven, J. A., Sá, J., Szlachetko, J. & Nachtegaal, M. (2012). *Chimia*, **66**, 699–705.

Abdul Rahman, M. B. B., Bolton, P. R., Evans, J., Dent, A. J., Harvey, I. & Diaz-Moreno, S. (2003). *Faraday Discuss.* **122**, 211–222.

Agostini, G., Lamberti, C., Pellegrini, R., Leofanti, G., Giannici, F., Longo, A. & Groppo, E. (2014). *ACS Catal.* **4**, 187–194.

Aksenov, V. L., Koval'chuk, M. V., Kuz'min, A. Y., Purans, Y. & Tyutyunnikov, S. I. (2006). *Crystallogr. Rep.* **51**, 908–935.

Allen, P. G., Conradson, S. D. & Penner-Hahn, J. E. (1993). *J. Appl. Cryst.* **26**, 172–179.

Allinson, N. M., Baker, G., Greaves, G. N. & Nicoll, J. K. (1988). *Nucl. Instrum. Methods Phys. Res. A*, **266**, 592–597.

Amakawa, K., Sun, L. L., Guo, C. S., Hävecker, M., Kube, P., Wachs, I. E., Lwin, S., Frenkel, A. I., Patlolla, A., Hermann, K., Schlögl, R. & Trunschke, A. (2013). *Angew. Chem. Int. Ed.* **52**, 13553–13557.

Andrews, J. C. & Weckhuysen, B. M. (2013). *ChemPhysChem*, **14**, 3655–3666.

Aramburo, L. R., Liu, Y. J., Tyliszczak, T., de Groot, F. M. F., Andrews, J. C. & Weckhuysen, B. M. (2013). *ChemPhysChem*, **14**, 496–499.

Baier, S., Rochet, A., Hofmann, G., Kraut, M. & Grunwaldt, J. D. (2015). *Rev. Sci. Instrum.* **86**, 065101.

Bare, S. R. & Ressler, T. (2009). *Adv. Catal.* **52**, 339–465.

Bare, S. R., Yang, N., Kelly, S. D., Mickelson, G. E. & Modica, F. S. (2007). *Catal. Today*, **126**, 18–26.

Bartlett, S. A., Moulin, J., Tromp, M., Reid, G., Dent, A. J., Cibin, G., McGuinness, D. S. & Evans, J. (2014). *ACS Catal.* **4**, 4201–4204.

Bartlett, S. A., Wells, P. P., Nachtegaal, M., Dent, A. J., Cibin, G., Reid, G., Evans, J. & Tromp, M. (2011). *J. Catal.* **284**, 247–258.

Baudelet, F., Kong, Q., Nataf, L., Cafun, J. D., Congeduti, A., Monza, A., Chagnot, S. & Itié, J.-P. (2011). *High Press. Res.* **31**, 136–139.

Beale, A. M., van der Eerden, A. M. J., Jacques, S. D. M., Leynaud, O., O'Brien, M. G., Meneau, F., Nikitenko, S., Bras, W. & Weckhuysen, B. M. (2006). *J. Am. Chem. Soc.* **128**, 12386–12387.

Beale, A. M., van der Eerden, A. M. J., Kervinen, K., Newton, M. A. & Weckhuysen, B. M. (2005). *Chem. Commun.* **2005**, 3015–3017.

Beek, W. van, Safonova, O. V., Wiker, G. & Emerich, H. (2011). *Phase Transit.* **84**, 726–732.

Bhattacharyya, D., Poswal, A. K., Jha, S. N., Sangeeta & Sabharwal, S. C. (2009). *Nucl. Instrum. Methods Phys. Res. A*, **609**, 286–293.

Bordiga, S., Groppo, E., Agostini, G., van Bokhoven, J. A. & Lamberti, C. (2013). *Chem. Rev.* **113**, 1736–1850.

Bordiga, S., Lamberti, C., Bonino, F., Travert, A. & Thibault-Starzyk, F. (2015). *Chem. Soc. Rev.* **44**, 7262–7341.

Borfecchia, E., Garino, C., Salassa, L. & Lamberti, C. (2013). *Phil. Trans. R. Soc. A*, **371**, 20120132.

Borfecchia, E., Groppo, E., Bordiga, S. & Lamberti, C. (2024). *Int. Tables Crystallogr. I*, ch. 8.10, 988–998.

Borfecchia, E., Lomachenko, K. A., Giordanino, F., Falsig, H., Beato, P., Soldatov, A. V., Bordiga, S. & Lamberti, C. (2015). *Chem. Sci.* **6**, 548–563.

Borfecchia, E., Maurelli, S., Gianolio, D., Groppo, E., Chiesa, M., Bonino, F. & Lamberti, C. (2012). *J. Phys. Chem. C*, **116**, 19839–19850.

Borfecchia, E., Mino, L., Groppo, E., Bordiga, S., Bugaev, A. L., Budnyk, A., Lomachenko, K. A., Guda, A. A., Soldatov, M. A., Soldatov, A. V. & Lamberti, C. (2017). *Morphological, Compositional, and Shape Control of Materials for Catalysis*, edited by P. Fornasiero & M. Cargnello, pp. 221–284. Amsterdam: Elsevier.

Boubnov, A., Carvalho, H. W. P., Doronkin, D. E., Günter, T., Gallo, E., Atkins, A. J., Jacob, C. R. & Grunwaldt, J. D. (2014). *J. Am. Chem. Soc.* **136**, 13006–13015.

Bras, W., Nikitenko, S., Portale, G., Beale, A., Eerden, A. & Detollenaere, D. (2010). *J. Phys. Conf. Ser.* **247**, 012047.

Bressler, C. & Chergui, M. (2004). *Chem. Rev.* **104**, 1781–1812.

Bressler, C. & Chergui, M. (2010). *Annu. Rev. Phys. Chem.* **61**, 263–282.

Briois, V., La Fontaine, C., Belin, S., Barthe, L., Moreno, T., Pinty, V., Carcy, A., Girardot, R. & Fonda, E. (2016). *J. Phys. Conf. Ser.* **712**, 012149.

Britz, A., Assefa, T. A., Galler, A., Gawelda, W., Diez, M., Zalden, P., Khakhulin, D., Fernandes, B., Gessler, P., Sotoudi Namin, H., Beckmann, A., Harder, M., Yavaş, H. & Bressler, C. (2016). *J. Synchrotron Rad.* **23**, 1409–1423.

Buurmans, I. L. C. & Weckhuysen, B. M. (2012). *Nat. Chem.* **4**, 873–886.

Cammarata, M., Bertoni, R., Lorenc, M., Cailleau, H., Di Matteo, S., Mauriac, C., Matar, S. F., Lemke, H., Chollet, M., Ravy, S., Laulhé, C., Létard, J. F. & Collet, E. (2014). *Phys. Rev. Lett.* **113**, 227402.

Canton, S. E., Kjaer, K. S., Vankó, G., van Driel, T. B., Adachi, S. I., Bordage, A., Bressler, C., Chabera, P., Christensen, M., Dohn, A. O., Galler, A., Gawelda, W., Gosztola, D., Haldrup, K., Harlang, T., Liu, Y. Z., Møller, K. B., Németh, Z., Nozawa, S., Pápai, M., Sato, T., Sato, T., Suarez-Alcantara, K., Togashi, T., Tono, K., Uhlig, J.,

Vithanage, D. A., Wärnmark, K., Yabashi, M., Zhang, J. X., Sundström, V. & Nielsen, M. M. (2015). *Nat. Commun.* **6**, 6359.
Cats, K. H., Gonzalez-Jimenez, I. D., Liu, Y. J., Nelson, J., van Campen, D., Meirer, F., van der Eerden, A. M. J., de Groot, F. M. F., Andrews, J. C. & Weckhuysen, B. M. (2013). *Chem. Commun.* **49**, 4622–4624.
Cezar, J. C., Souza-Neto, N. M., Piamonteze, C., Tamura, E., Garcia, F., Carvalho, E. J., Neueschwander, R. T., Ramos, A. Y., Tolentino, H. C. N., Caneiro, A., Massa, N. E., Martinez-Lope, M. J., Alonso, J. A. & Itié, J.-P. (2010). *J. Synchrotron Rad.* **17**, 93–102.
Chen, J. G. (1997). *Surf. Sci. Rep.* **30**, 1–152.
Chen, L. X. (2004). *Angew. Chem. Int. Ed.* **43**, 2886–2905.
Chen, L. X., Zhang, X. & Shelby, M. L. (2014). *Chem. Sci.* **5**, 4136–4152.
Chen, L. X., Zhang, X., Lockard, J. V., Stickrath, A. B., Attenkofer, K., Jennings, G. & Liu, D.-J. (2010). *Acta Cryst.* A**66**, 240–251.
Chupas, P. J., Chapman, K. W., Kurtz, C., Hanson, J. C., Lee, P. L. & Grey, C. P. (2008). *J. Appl. Cryst.* **41**, 822–824.
Clausen, B. S., Steffensen, G., Fabius, B., Villadsen, J., Feidenhans'l, R. & Topsøe, H. (1991). *J. Catal.* **132**, 524–535.
Cotte, M., Fabris, T., Agostini, G., Motta Meira, D., De Viguerie, L. & Solé, V. A. (2016). *Anal. Chem.* **88**, 6154–6160.
Couves, J. W., Thomas, J. M., Waller, D., Jones, R. H., Dent, A. J., Derbyshire, G. E. & Greaves, G. N. (1991). *Nature*, **354**, 465–468.
D'Acapito, F., Boscherini, F., Marcelli, A. & Mobilio, S. (1992). *Rev. Sci. Instrum.* **63**, 899–901.
Dartyge, E., Depautex, C., Dubuisson, J. M., Fontaine, A., Jucha, A., Leboucher, P. & Tourillon, G. (1986). *Nucl. Instrum. Methods Phys. Res. A*, **246**, 452–460.
Dent, A., Evans, J., Newton, M., Corker, J., Russell, A., Abdul Rahman, M. B., Fiddy, S., Mathew, R., Farrow, R., Salvini, G. & Atkinson, P. (1999). *J. Synchrotron Rad.* **6**, 381–383.
Dent, A. J., Cibin, G., Ramos, S., Parry, S. A., Gianolio, D., Smith, A. D., Scott, S. M., Varandas, L., Patel, S., Pearson, M. R., Hudson, L., Krumpa, N. A., Marsch, A. S. & Robbins, P. E. (2013). *J. Phys. Conf. Ser.* **430**, 012023.
Dent, A. J., Wells, M. P., Farrow, R. C., Ramsdale, C. A., Derbyshire, G. E., Greaves, G. N., Couves, J. W. & Thomas, J. M. (1992). *Rev. Sci. Instrum.* **63**, 903–906.
Diaz-Moreno, S., Hayama, S., Amboage, M., Freeman, A., Sutter, J. & Duller, G. (2009). *J. Phys. Conf. Ser.* **190**, 012038.
Doronkin, D. E., Casapu, M., Günter, T., Müller, O., Frahm, R. & Grunwaldt, J. D. (2014). *J. Phys. Chem. C*, **118**, 10204–10212.
Doronkin, D. E., Lichtenberg, H. & Grunwaldt, J.-D. (2017). *XAFS Techniques for Catalysts, Nanomaterials, and Surfaces*, edited by Y. Iwasawa, K. Asakura & M. Tada, pp. 75–89. Cham: Springer.
Ellis, P. J., Fairlamb, I. J. S., Hackett, S. F. J., Wilson, K. & Lee, A. F. (2010). *Angew. Chem. Int. Ed.* **49**, 1820–1824.
Escudero, C., Jiang, P., Pach, E., Borondics, F., West, M. W., Tuxen, A., Chintapalli, M., Carenco, S., Guo, J. & Salmeron, M. (2013). *J. Synchrotron Rad.* **20**, 504–508.
Fiddy, S. G., Newton, M. A., Corker, J. M., Turin, S., Campbell, T., Evans, J., Dent, A. J. & Salvini, G. (1999). *Chem. Commun.* **1999**, 851–852.
Figueroa, S. J. A., Gibson, D., Mairs, T., Pasternak, S., Newton, M. A., Di Michiel, M., Andrieux, J., Christoforidis, K. C., Iglesias-Juez, A., Fernández-García, M. & Prestipino, C. (2013). *J. Appl. Cryst.* **46**, 1523–1527.
Figueroa, S. J. A. & Prestipino, C. (2016). *J. Phys. Conf. Ser.* **712**, 012012.
Flank, A. M., Fontaine, A., Jucha, A., Lemonnier, M., Raoux, D. & Williams, C. (1983). *Nucl. Instrum. Methods Phys. Res.* **208**, 651–654.
Flank, A. M., Fontaine, A., Jucha, A., Lemonnier, M. & Williams, C. (1982). *J. Phys. Lett.* **43**, 315–319.
Fonda, E., Rochet, A., Ribbens, M., Barthe, L., Belin, S. & Briois, V. (2012). *J. Synchrotron Rad.* **19**, 417–424.
Frahm, R. (1988). *Nucl. Instrum. Methods Phys. Res. A*, **270**, 578–581.
Frenkel, A. I., Rodriguez, J. A. & Chen, J. G. G. (2012). *ACS Catal.* **2**, 2269–2280.
Frenkel, A. I., Wang, Q., Marinkovic, N., Chen, J. G., Barrio, L., Si, R., Cámara, A. L., Estrella, A. M., Rodriguez, J. A. & Hanson, J. C. (2011). *J. Phys. Chem. C*, **115**, 17884–17890.
Fulton, J. L., Linehan, J. C., Autrey, T., Balasubramanian, M., Chen, Y. & Szymczak, N. K. (2007). *J. Am. Chem. Soc.* **129**, 11936–11949.
Gamarra, D., Belver, C., Fernández-García, M. & Martínez-Arias, A. (2007). *J. Am. Chem. Soc.* **129**, 12064–12065.
Gamarra, D., Fernández-García, M., Belver, C. & Martínez-Arias, A. (2010). *J. Phys. Chem. C*, **114**, 18576–18582.
Gomez-Hens, A. & Perez-Bendito, D. (1991). *Anal. Chim. Acta*, **242**, 147–177.
Gonzalez-Jimenez, I. D., Cats, K., Davidian, T., Ruitenbeek, M., Meirer, F., Liu, Y. J., Nelson, J., Andrews, J. C., Pianetta, P., de Groot, F. M. F. & Weckhuysen, B. M. (2012). *Angew. Chem. Int. Ed.* **51**, 11986–11990.
Göries, D., Dicke, B., Roedig, P., Stübe, N., Meyer, J., Galler, A., Gawelda, W., Britz, A., Gessler, P., Sotoudi Namin, H., Beckmann, A., Schlie, M., Warmer, M., Naumova, M., Bressler, C., Rübhausen, M., Weckert, E. & Meents, A. (2016). *Rev. Sci. Instrum.* **87**, 053116.
Groppo, E., Agostini, G., Borfecchia, E., Wei, L., Giannici, F., Portale, G., Longo, A. & Lamberti, C. (2014). *J. Phys. Chem. C*, **118**, 8406–8415.
Groppo, E., Agostini, G., Piovano, A., Muddada, N. B., Leofanti, G., Pellegrini, R., Portale, G., Longo, A. & Lamberti, C. (2012). *J. Catal.* **287**, 44–54.
Groppo, E., Uddin, M. J., Bordiga, S., Zecchina, A. & Lamberti, C. (2008). *Angew. Chem. Int. Ed.* **47**, 9269–9273.
Grunwaldt, J.-D., Caravati, M., Hannemann, S. & Baiker, A. (2004). *Phys. Chem. Chem. Phys.* **6**, 3037–3047.
Grunwaldt, J.-D. & Clausen, B. S. (2002). *Top. Catal.* **18**, 37–43.
Grunwaldt, J.-D., Hannemann, S., Gttlicher, J., Mangold, S., Denecke, M. A. & Baiker, A. (2005). *Phys. Scr.* **2005**, 769.
Grunwaldt, J.-D. & Schroer, C. G. (2010). *Chem. Soc. Rev.* **39**, 4741–4753.
Grunwaldt, J.-D., Wagner, J. B. & Dunin-Borkowski, R. E. (2013). *ChemCatChem*, **5**, 62–80.
Guilera, G., Gorges, B., Pascarelli, S., Vitoux, H., Newton, M. A., Prestipino, C., Nagai, Y. & Hara, N. (2009). *J. Synchrotron Rad.* **16**, 628–634.
Guilera, G., Newton, M. A., Polli, C., Pascarelli, S., Guino, M. & Hii, K. K. (2006). *Chem. Commun.* **2006**, 4306–4308.
Günter, T., Doronkin, D. E., Boubnov, A., Carvalho, H. W. P., Casapu, M. & Grunwaldt, J. D. (2016). *Top. Catal.* **59**, 866–874.
Hagelstein, M., Cunis, S., Frahm, R., Niemann, W. & Rabe, P. (1989). *Physica B*, **158**, 324–325.
Hagelstein, M., Ferrero, C., Hatje, U., Ressler, T. & Metz, W. (1995). *J. Synchrotron Rad.* **2**, 174–180.
Hannemann, S., Grunwaldt, J. D., Kimmerle, B., Baiker, A., Boye, P. & Schroer, C. (2009). *Top. Catal.* **52**, 1360–1370.
Hannemann, S., Grunwaldt, J. D., van Vegten, N., Baiker, A., Boye, P. & Schroer, C. G. (2007). *Catal. Today*, **126**, 54–63.
Harmand, M., Coffee, R., Bionta, M. R., Chollet, M., French, D., Zhu, D., Fritz, D. M., Lemke, H. T., Medvedev, N., Ziaja, B., Toleikis, S. & Cammarata, M. (2013). *Nat. Photon.* **7**, 215–218.
Hävecker, M., Cavalleri, M., Herbert, R., Follath, R., Knop-Gericke, A., Hess, C., Hermann, K. & Schlögl, R. (2009). *Phys. Status Solidi B*, **246**, 1459–1469.
Hübner, M., Koziej, D., Bauer, M., Barsan, N., Kvashnina, K., Rossell, M. D., Weimar, U. & Grunwaldt, J. D. (2011). *Angew. Chem. Int. Ed.* **50**, 2841–2844.
Inada, Y., Hayashi, H., Funahashi, S. & Nomura, M. (1997). *Rev. Sci. Instrum.* **68**, 2973–2977.
Ishikawa, T., Aoyagi, H., Asaka, T., Asano, Y., Azumi, N., Bizen, T., Ego, H., Fukami, K., Fukui, T., Furukawa, Y., Goto, S., Hanaki, H., Hara, T., Hasegawa, T., Hatsui, T., Higashiya, A., Hirono, T., Hosoda, N., Ishii, M., Inagaki, T., Inubushi, Y., Itoga, T., Joti, Y.,

Kago, M., Kameshima, T., Kimura, H., Kirihara, Y., Kiyomichi, A., Kobayashi, T., Kondo, C., Kudo, T., Maesaka, H., Maréchal, X. M., Masuda, T., Matsubara, S., Matsumoto, T., Matsushita, T., Matsui, S., Nagasono, M., Nariyama, N., Ohashi, H., Ohata, T., Ohshima, T., Ono, S., Otake, Y., Saji, C., Sakurai, T., Sato, T., Sawada, K., Seike, T., Shirasawa, K., Sugimoto, T., Suzuki, S., Takahashi, S., Takebe, H., Takeshita, K., Tamasaku, K., Tanaka, H., Tanaka, R., Tanaka, T., Togashi, T., Togawa, K., Tokuhisa, A., Tomizawa, H., Tono, K., Wu, S., Yabashi, M., Yamaga, M., Yamashita, A., Yanagida, K., Zhang, C., Shintake, T., Kitamura, H. & Kumagai, N. (2012). *Nat. Photon.* **6**, 540–544.

Jacques, S. D. M., Leynaud, O., Strusevich, D., Stukas, P., Barnes, P., Sankar, G., Sheehy, M., O'Brien, M. G., Iglesias-Juez, A. & Beale, A. M. (2009). *Catal. Today*, **145**, 204–212.

Janssens, T. V. W., Falsig, H., Lundegaard, L. F., Vennestrøm, P. N. R., Rasmussen, S. B., Moses, P. G., Giordanino, F., Borfecchia, E., Lomachenko, K. A., Lamberti, C., Bordiga, S., Godiksen, A., Mossin, S. & Beato, P. (2015). *ACS Catal.* **5**, 2832–2845.

Jennings, G., Jäger, W. J. H. & Chen, L. X. (2002). *Rev. Sci. Instrum.* **73**, 362–368.

Jian, R. S., Huang, R. X. & Lu, C. J. (2012). *Talanta*, **88**, 160–167.

Kalirai, S., Boesenberg, U., Falkenberg, G., Meirer, F. & Weckhuysen, B. M. (2015). *ChemCatChem*, **7**, 3674–3682.

Kaminaga, U., Matsushita, T. & Kohra, K. (1981). *Jpn. J. Appl. Phys.* **20**, L355–L358.

Khalid, S., Ehrlich, S. N., Lenhard, A. & Clay, B. (2011). *Nucl. Instrum. Methods Phys. Res. A*, **649**, 64–66.

Kilcoyne, A. L. D., Tyliszczak, T., Steele, W. F., Fakra, S., Hitchcock, P., Franck, K., Anderson, E., Harteneck, B., Rightor, E. G., Mitchell, G. E., Hitchcock, A. P., Yang, L., Warwick, T. & Ade, H. (2003). *J. Synchrotron Rad.* **10**, 125–136.

Kimmerle, B., Grunwaldt, J. D., Baiker, A., Glatzel, P., Boye, P., Stephan, S. & Schroer, C. G. (2009). *J. Phys. Chem. C*, **113**, 3037–3040.

Kornienko, N., Resasco, J., Becknell, N., Jiang, C. M., Liu, Y. S., Nie, K. Q., Sun, X. H., Guo, J. H., Leone, S. R. & Yang, P. D. (2015). *J. Am. Chem. Soc.* **137**, 7448–7455.

Kristiansen, P. T., Rocha, T. C. R., Knop-Gericke, A., Guo, J. H. & Duda, L. C. (2013). *Rev. Sci. Instrum.* **84**, 113107.

Lamberti, C., Bordiga, S., Bonino, F., Prestipino, C., Berlier, G., Capello, L., D'Acapito, F., Llabrés i Xamena, F. X. & Zecchina, A. (2003). *Phys. Chem. Chem. Phys.* **5**, 4502–4509.

Lamberti, C., Borfecchia, E., van Bokhoven, J. A. & Fernández-García, M. (2016). *X-ray Absorption and X-ray Emission Spectroscopy: Theory and Applications*, edited by J. A. van Bokhoven & C. Lamberti, pp. 303–350. Chichester: John Wiley & Sons.

Lamberti, C., Prestipino, C., Bonino, F., Capello, L., Bordiga, S., Spoto, G., Zecchina, A., Diaz Moreno, S., Cremaschi, B., Garilli, M., Marsella, A., Carmello, D., Vidotto, S. & Leofanti, G. (2002). *Angew. Chem. Int. Ed.* **41**, 2341–2344.

Lamberti, C., Prestipino, C., Bordiga, S., Berlier, G., Spoto, G., Zecchina, A., Laloni, A., La Manna, F., D'Anca, F., Felici, R., D'Acapito, F. & Roy, P. (2003). *Nucl. Instrum. Methods Phys. Res. B*, **200**, 196–201.

Lamberti, C., Turnes Palomino, G., Bordiga, S., Berlier, G., D'Acapito, F. & Zecchina, A. (2000). *Angew. Chem. Int. Ed.* **39**, 2138–2141.

Lamberti, C. & van Bokhoven, J. A. (2016). *X-ray Absorption and X-ray Emission Spectroscopy: Theory and Applications*, edited by J. A. van Bokhoven & C. Lamberti, pp. 353–383. Chichester: John Wiley & Sons.

Lamberti, C., Zecchina, A., Groppo, E. & Bordiga, S. (2010). *Chem. Soc. Rev.* **39**, 4951–5001.

Lee, P. L., Beno, M. A., Jennings, G., Ramanathan, M., Knapp, G. S., Huang, K., Bai, J. & Montano, P. A. (1994). *Rev. Sci. Instrum.* **65**, 1–6.

Leofanti, G., Marsella, A., Cremaschi, B., Garilli, M., Zecchina, A., Spoto, G., Bordiga, S., Fisicaro, P., Berlier, G., Prestipino, C., Casali, G. & Lamberti, C. (2001). *J. Catal.* **202**, 279–295.

Leofanti, G., Marsella, A., Cremaschi, B., Garilli, M., Zecchina, A., Spoto, G., Bordiga, S., Fisicaro, P., Prestipino, C., Villain, F. & Lamberti, C. (2002). *J. Catal.* **205**, 375–381.

Lesage, T., Verrier, C., Bazin, P., Saussey, J. & Daturi, M. (2003). *Phys. Chem. Chem. Phys.* **5**, 4435–4440.

Lima, F. A., Milne, C. J., Amarasinghe, D. C. V., Rittmann-Frank, M. H., van der Veen, R. M., Reinhard, M., Pham, V. T., Karlsson, S., Johnson, S. L., Grolimund, D., Borca, C., Huthwelker, T., Janousch, M., van Mourik, F., Abela, R. & Chergui, M. (2011). *Rev. Sci. Instrum.* **82**, 063111.

Liu, Y., Meirer, F., Krest, C. M., Webb, S. & Weckhuysen, B. M. (2016). *Nat. Commun.* **7**, 12634.

Liu, Y., Meirer, F., Williams, P. A., Wang, J., Andrews, J. C. & Pianetta, P. (2012). *J. Synchrotron Rad.* **19**, 281–287.

Lomachenko, K. A., Borfecchia, E., Negri, C., Berlier, G., Lamberti, C., Beato, P., Falsig, H. & Bordiga, S. (2016). *J. Am. Chem. Soc.* **138**, 12025–12028.

March, A. M., Stickrath, A., Doumy, G., Kanter, E. P., Krässig, B., Southworth, S. H., Attenkofer, K., Kurtz, C. A., Chen, L. X. & Young, L. (2011). *Rev. Sci. Instrum.* **82**, 073110.

Martinez-Criado, G., Borfecchia, E., Mino, L. & Lamberti, C. (2013). *Characterization of Semiconductor Heterostructures and Nanostructures II*, edited by C. Lamberti & G. Agostini, pp. 361–412. Amsterdam: Elsevier.

Mathon, O., Beteva, A., Borrel, J., Bugnazet, D., Gatla, S., Hino, R., Kantor, I., Mairs, T., Munoz, M., Pasternak, S., Perrin, F. & Pascarelli, S. (2015). *J. Synchrotron Rad.* **22**, 1548–1554.

Mathon, O., Kantor, I. & Pascarelli, S. (2016). *X-ray Absorption and X-ray Emission Spectroscopy: Theory and Applications*, edited by J. A. van Bokhoven & C. Lamberti, pp. 185–212. Chichester: John Wiley & Sons.

Matsushita, T. & Phizackerley, R. P. (1981). *Jpn. J. Appl. Phys.* **20**, 2223–2228.

Meirer, F., Kalirai, S., Morris, D., Soparawalla, S., Liu, Y., Mesu, G., Andrews, J. C. & Weckhuysen, B. M. (2015). *Sci. Adv.* **1**, e1400199.

Meirer, F., Kalirai, S., Weker, J. N., Liu, Y., Andrews, J. C. & Weckhuysen, B. M. (2015). *Chem. Commun.* **51**, 8097–8100.

Meirer, F., Morris, D. T., Kalirai, S., Liu, Y. J., Andrews, J. C. & Weckhuysen, B. M. (2015). *J. Am. Chem. Soc.* **137**, 102–105.

Meitzner, G., Bare, S. R., Parker, D., Woo, H. & Fischer, D. A. (1998). *Rev. Sci. Instrum.* **69**, 2618–2621.

Meneau, F., Sankar, G., Morgante, N., Winter, R., Catlow, C. R. A., Greaves, G. N. & Thomas, J. M. (2003). *Faraday Discuss.* **122**, 203–210.

Meunier, F. C. (2010). *Chem. Soc. Rev.* **39**, 4602–4614.

Milne, C. J., Penfold, T. J. & Chergui, M. (2014). *Coord. Chem. Rev.* **277–278**, 44–68.

Mino, L., Borfecchia, E., Segura-Ruiz, J., Giannini, C., Martinez-Criado, G. & Lamberti, C. (2018). *Rev. Mod. Phys.* **90**, 025007.

Muddada, N. B., Olsbye, U., Caccialupi, L., Cavani, F., Leofanti, G., Gianolio, D., Bordiga, S. & Lamberti, C. (2010). *Phys. Chem. Chem. Phys.* **12**, 5605–5618.

Muddada, N. B., Olsbye, U., Leofanti, G., Gianolio, D., Bonino, F., Bordiga, S., Fuglerud, T., Vidotto, S., Marsella, A. & Lamberti, C. (2010). *Dalton Trans.* **39**, 8437–8449.

Müller, O., Lützenkirchen-Hecht, D. & Frahm, R. (2015). *Rev. Sci. Instrum.* **86**, 093905.

Müller, O., Nachtegaal, M., Just, J., Lützenkirchen-Hecht, D. & Frahm, R. (2016). *J. Synchrotron Rad.* **23**, 260–266.

Nachtegaal, M., Müller, O., König, C. & Frahm, R. (2016). *X-ray Absorption and X-ray Emission Spectroscopy: Theory and Applications*, edited by J. A. van Bokhoven & C. Lamberti, pp. 155–183. Chichester: John Wiley & Sons.

Nagai, Y., Dohmae, K., Ikeda, Y., Takagi, N., Tanabe, T., Hara, N., Guilera, G., Pascarelli, S., Newton, M. A., Kuno, O., Jiang, H. Y., Shinjoh, H. & Matsumoto, S. (2008). *Angew. Chem. Int. Ed.* **47**, 9303–9306.

Newton, M. A., Brazier, J. B., Barreiro, E. M., Parry, S., Emmerich, H., Adrio, L. A., Mulligan, C. J., Hellgardt, K. & Hii, K. K. (2016). *Green Chem.* **18**, 406–411.
Newton, M. A., Dent, A. J., Diaz-Moreno, S., Fiddy, S. G., Jyoti, B. & Evans, J. (2003). *Chem. Commun.* **2003**, 1906–1907.
Newton, M. A., Dent, A. J. & Evans, J. (2002). *Chem. Soc. Rev.* **31**, 83–95.
Newton, M. A., Jyoti, B., Dent, A. J., Fiddy, S. G. & Evans, J. (2004). *Chem. Commun.* **2004**, 2382–2383.
Newton, M. A. & van Beek, W. (2010). *Chem. Soc. Rev.* **39**, 4845–4863.
Nikitenko, S., Beale, A. M., van der Eerden, A. M. J., Jacques, S. D. M., Leynaud, O., O'Brien, M. G., Detollenaere, D., Kaptein, R., Weckhuysen, B. M. & Bras, W. (2008). *J. Synchrotron Rad.* **15**, 632–640.
Oyanagi, H., Matsushita, T., Kaminaga, U. & Hashimoto, H. (1986). *J. Phys. Colloq.* **47**, C8-139–C8-142.
Oyanagi, H., Sun, Z. H., Jiang, Y., Uehara, M., Nakamura, H., Yamashita, K., Zhang, L., Lee, C., Fukano, A. & Maeda, H. (2011). *J. Synchrotron Rad.* **18**, 272–279.
Paolucci, C., Parekh, A. A., Khurana, I., Di Iorio, J. R., Li, H., Albarracin Caballero, J. D., Shih, A. J., Anggara, T., Delgass, W. N., Miller, J. T., Ribeiro, F. H., Gounder, R. & Schneider, W. F. (2016). *J. Am. Chem. Soc.* **138**, 6028–6048.
Pascarelli, S., Mathon, O., Mairs, T., Kantor, I., Agostini, G., Strohm, C., Pasternak, S., Perrin, F., Berruyer, G., Chappelet, P., Clavel, C. & Dominguez, M. C. (2016). *J. Synchrotron Rad.* **23**, 353–368.
Pascarelli, S., Neisius, T. & De Panfilis, S. (1999). *J. Synchrotron Rad.* **6**, 1044–1050.
Patlolla, A., Carino, E. V., Ehrlich, S. N., Stavitski, E. & Frenkel, A. I. (2012). *ACS Catal.* **2**, 2216–2223.
Pellegrini, R., Agostini, G., Groppo, E., Piovano, A., Leofanti, G. & Lamberti, C. (2011). *J. Catal.* **280**, 150–160.
Phizackerley, R. P., Rek, Z. U., Stephenson, G. B., Conradson, S. D., Hodgson, K. O., Matsushita, T. & Oyanagi, H. (1983). *J. Appl. Cryst.* **16**, 220–232.
Poo-arporn, Y., Chirawatkul, P., Saengsui, W., Chotiwan, S., Kityakarn, S., Klinkhieo, S., Hormes, J. & Songsiriritthigul, P. (2012). *J. Synchrotron Rad.* **19**, 937–943.
Prestipino, C., Mathon, O., Hino, R., Beteva, A. & Pascarelli, S. (2011). *J. Synchrotron Rad.* **18**, 176–182.
Price, S. W. T., Geraki, K., Ignatyev, K., Witte, P. T., Beale, A. M. & Mosselmans, J. F. W. (2015). *Angew. Chem. Int. Ed.* **54**, 9886–9889.
Price, S. W. T., Ignatyev, K., Geraki, K., Basham, M., Filik, J., Vo, N. T., Witte, P. T., Beale, A. M. & Mosselmans, J. F. W. (2015). *Phys. Chem. Chem. Phys.* **17**, 521–529.
Rabeah, J., Radnik, J., Briois, V., Maschmeyer, D., Stochniol, G., Peitz, S., Reeker, H., La Fontaine, C. & Brückner, A. (2016). *ACS Catal.* **6**, 8224–8228.
Richwin, M., Zaeper, R., Lützenkirchen-Hecht, D. & Frahm, R. (2001). *J. Synchrotron Rad.* **8**, 354–356.
Ruffoni, M. P. & Pettifer, R. F. (2006). *J. Synchrotron Rad.* **13**, 489–493.
Saigo, S., Oyanagi, H., Matsushita, T., Hashimoto, H., Yoshida, N., Fujimoto, M. & Nagamura, T. (1986). *J. Phys. Colloq.* **47**, C8-555–C8-561.
Sankar, G., Cao, E. H. & Gavriilidis, A. (2007). *Catal. Today*, **125**, 24–28.
Sato, T., Nozawa, S., Ichiyanagi, K., Tomita, A., Chollet, M., Ichikawa, H., Fujii, H., Adachi, S. & Koshihara, S. (2009). *J. Synchrotron Rad.* **16**, 110–115.
Smit, E. de, Swart, I., Creemer, J. F., Hoveling, G. H., Gilles, M. K., Tyliszczak, T., Kooyman, P. J., Zandbergen, H. W., Morin, C., Weckhuysen, B. M. & de Groot, F. M. F. (2008). *Nature*, **456**, 222–225.
Smolentsev, G., Guda, A., Zhang, X. Y., Haldrup, K., Andreiadis, E. S., Chavarot-Kerlidou, M., Canton, S. E., Nachtegaal, M., Artero, V. & Sundstrom, V. (2013). *J. Phys. Chem. C*, **117**, 17367–17375.
Smolentsev, G., Guilera, G., Tromp, M., Pascarelli, S. & Soldatov, A. V. (2009). *J. Chem. Phys.* **130**, 174508.
Somorjai, G. A., Beaumont, S. K. & Alayoglu, S. (2011). *Angew. Chem. Int. Ed.* **50**, 10116–10129.
Suzuki, Y. & Terada, Y. (2016). *X-ray Absorption and X-ray Emission Spectroscopy: Theory and Applications*, edited by J. A. van Bokhoven & C. Lamberti, pp. 251–279. Chichester: John Wiley & Sons.
Tada, M., Ishiguro, N., Uruga, T., Tanida, H., Terada, Y., Nagamatsu, S., Iwasawa, Y. & Ohkoshi, S. (2011). *Phys. Chem. Chem. Phys.* **13**, 14910–14913.
Tada, M., Murata, S., Asakoka, T., Hiroshima, K., Okumura, K., Tanida, H., Uruga, T., Nakanishi, H., Matsumoto, S., Inada, Y., Nomura, M. & Iwasawa, Y. (2007). *Angew. Chem. Int. Ed.* **46**, 4310–4315.
Tamenori, Y. (2013). *J. Synchrotron Rad.* **20**, 419–425.
Terada, Y., Tanida, H., Uruga, T., Takeuchi, A., Suzuki, Y., Goto, S., McNulty, I., Eyberger, C. & Lai, B. (2011). *AIP Conf. Proc.* **1365**, 172–175.
Thomas, J. M. (1997). *Chem. Eur. J.* **3**, 1557–1562.
Tibiletti, D., Amieiro-Fonseca, A., Burch, R., Chen, Y., Fisher, J. M., Goguet, A., Hardacre, C., Hu, P. & Thompsett, A. (2005). *J. Phys. Chem. B*, **109**, 22553–22559.
Toyoshima, R. & Kondoh, H. (2015). *J. Phys. Condens. Matter*, **27**, 083003.
Uruga, T., Tanida, H., Inoue, K., Yamazaki, H. & Irie, T. (2007). *AIP Conf. Proc.* **882**, 914–916.
Valenzano, L., Vitillo, J. G., Chavan, S., Civalleri, B., Bonino, F., Bordiga, S. & Lamberti, C. (2012). *Catal. Today*, **182**, 67–79.
Xu, M. J., Tang, Z. T., Duan, Y. X. & Liu, Y. (2016). *Crit. Rev. Anal. Chem.* **46**, 291–304.
Yao, S. Y., Mudiyanselage, K., Xu, W. Q., Johnston-Peck, A. C., Hanson, J. C., Wu, T. P., Stacchiola, D., Rodriguez, J. A., Zhao, H. Y., Beyer, K. A., Chapman, K. W., Chupas, P. J., Martínez-Arias, A., Si, R., Bolin, T. B., Liu, W. J. & Senanayake, S. D. (2014). *ACS Catal.* **4**, 1650–1661.